Proceedings of the 2006 WSEAS/IASME International Conference on Fluid Mechanics, Miami, Florida, USA, January 18-20, 2006 (pp89-94)

Computational Investigations of Jet Aspect Ratio Effects in Turbulent Film Cooling at Different Injection Angles

SHADI MAHJOOB, MOHAMMAD TAEIBI-RAHNI, KHODAYAR JAVADI, ELHAM TOLOUEI
Aerospace Research Institute
Ministry of Science, Research, and Technology
Havafaza Alley, Mahestan St., Iranzamin St., Shahrak Ghods, Tehran , P.O.Box:14665-834, I.R.IRAN

Abstract: Blade film cooling is one of the best methods to improve the efficiency of gas turbines. As a fundamental study, the effects of jet aspect ratio are numerically simulated here at jet injection angles of 30° and 90° and velocity ratio of 0.5. Incompressible, stationary, viscous, turbulent flow is assumed. For simulation of jet injection angle of 30°, the STAR-CD CFD software with standard $k-\varepsilon$ model is used. For simulation of jet injection angle of 90°, a software is developed by authors (CFDARI), which uses Reynolds stress model (RSM) for turbulence modeling. Both of these codes use a cell centered finite volume method on a non-uniform structured staggered grid. The jet flow Reynolds number, based on the jet's hydraulic diameter, was 4700. The study of jet aspect ratio shows that, stretching the hole in spanwise direction increases the film cooling effectiveness. In addition at the injection angle of 30°, the more the rectangular section stretches in spanwise direction, the more rapidly the cooling effectiveness increases.

Key-Words: Film Cooling, Gas Turbine, Computational Fluid Dynamics, Jet Aspect Ratio, Jet Injection Angle

Nomenclature

D	Side of the Jet Exit (0.0127m)
R	Velocity Ratio (V_{Jet}/V_{CF})
η	Film Cooling Effectiveness; $(T_{AW}-T_{CF})/(T_{Jet}-T_{CF})$
θ	Film Cooling Efficiency; $(T-T_{CF})/(T_{Jet}-T_{CF})$
$(\,)_{CF,\,Jet}$	Designates Cross Flow and Jet, respectively
$(\,)_{AW}$	Designates Adiabatic Wall

1 Introduction

One of the best methods to improve the jet engine efficiency is to increase the turbine entrance temperature. However, this temperature is limited by the potential structural failure of the engine components, especially, the first stage of the turbine blades. The cooling air reduces the capacity of the turbine to drive the compressor, because of the lower temperature at which it enters the turbine. Furthermore, the cooling air mixes with the mainstream turbine air and causes aerodynamic losses. Both of these effects are so strong that, vigorous steps are taken to minimize them [1].

In film cooling, cool air is injected into the cross flow very near the surface through some rows of slot or discrete holes. Since, in slot injection film cooling, the cooling jet is injected all along the span, it results in a better performance. However, because of structural considerations, rows of discrete film cooling holes are usually used. Film cooling with discrete holes has problems like non-uniformity of cooling in spanwise direction and excessive penetration of the cooling jets into the main stream. To overcome these difficulties, rows of rectangular or expanded-shape holes are mostly used in more recent years [2].

Gartshore et al. [3] studied the effects of two different hole-shapes (circular and squared). Their results show that, the squared holes are slightly superior (from cooling point of view) only very close to the injection point and only at low velocity ratios, e.g., R=0.5. Note, many people have compared expanded-shape and circular cross sectional film cooling holes, while only a few have compared squared and rectangular film cooling holes.

Muldoon and Acharya [4] and Licu et al. [5] investigated flow characteristics and film cooling performance downstream of rectangular holes, using numerical and experimental methods, respectively. Cho et al. [2] studied film cooling using jet injection angle of 90° with squared and rectangular holes. They investigated local heat transfer characteristics inside the holes with variations of the blowing ratio and the jet Reynolds number. Although, film cooling offers an excellent compromise between the protection of the walls and the aerodynamic efficiency, it can even be ineffective if the related parameters are not chosen properly.

2 Computational Geometric and Grid

The computational domain used was a 45D×25D×4.5D cube with a 1D×1D jet channel, shown in Fig. 1(a). Three different cases of jet exit cross sections were used in this study (Fig. 1b). These dimensions were chosen such that, the jet Reynolds number stayed the same (4700). Note, in all cases studied, the distance between the main inflow boundary to the beginning of the jet is set to 4.5D and the depth of the jet channel was taken to be 5D.

A 210,000 cell, non-uniform structured grid was used (Fig1a). Since, the flow complexity and the jet into cross flow interactions occur mostly near the wall (especially over and behind the jet), the grid was clustered there in Y direction, as well as at the jet exit in X and Z directions.

3 Flow Characteristics

The turbulent flow considered was assumed to be incompressible and stationary. The cooling jet velocity was taken to be 5.5 m/s and the jet flow Reynolds number, based on the jet's hydraulic diameter, was 4700. The velocity ratio (R) was 0.5. The thickness of

the boundary layer was estimated from the experimental results of Ajersch et al. [6] and was about 2D. The temperature of the cross and the jet flows were 1000K and 300K, respectively. Also, the density and the viscosity coefficient were 1.204 Kg/m^3 and 1.7894×10^{-5}, respectively.

4 Governing Equations

In this study, the following forms of the governing equations including continuity, momentum, and energy, were used:

$$\frac{\partial}{\partial x_i}(u_i) = 0,$$

$$\rho \frac{\partial}{\partial x_j}(u_i u_j) = -\frac{\partial p}{\partial x_i} + \frac{\partial \tau_{ij}}{\partial x_j} + \rho g_i + F_i,$$

$$\rho \frac{\partial}{\partial x_i}(u_i h) = \frac{\partial}{\partial x_i}\left[K \frac{\partial T}{\partial x_i}\right] + u_i \frac{\partial p}{\partial x_i} + \tau_{ij} \frac{\partial u_i}{\partial x_j},$$

$$\tau_{ij} = \left[\mu_{eff}\left(\frac{\partial u_i}{\partial x_j} + \frac{\partial u_j}{\partial x_i}\right)\right], \quad \mu_{eff} = \mu + \mu_T.$$

4.1 Turbulence Modeling

In order to study the jet aspect ratio, the standard $k-\varepsilon$ model was used at the optimal jet injection angle of 30°. The turbulent kinetic energy, k, and its rate of dissipation, ε, were obtained from the following transport equations, proposed by Jones and Launder [7]:

$$\rho\frac{Dk}{Dt} = \frac{\partial}{\partial x_i}\left[\left(\mu + \frac{\mu_t}{\sigma_k}\right)\frac{\partial k}{\partial x_i}\right] + G_k - \rho\varepsilon,$$

$$\rho\frac{D\varepsilon}{Dt} = \frac{\partial}{\partial x_i}\left[\left(\mu + \frac{\mu_t}{\sigma_\varepsilon}\right)\frac{\partial \varepsilon}{\partial x_i}\right] + C_{1\varepsilon}\frac{\varepsilon}{k}(G_k) - C_{2\varepsilon}\rho\frac{\varepsilon^2}{k}.$$

In addition, the standard wall functions, based on the work of Launder and Spalding [8] were used. Note, the standard $k-\varepsilon$ model can not predict complicated flows with excessive rate of strain (e.g. highly vortical flows), and with multiple length scales. On the other hand, our problem (with the jet injection angle of 90) is a very complicated flow, and thus eddy viscosity models are not very suitable. Therefore, Reynolds stress models (RSM) which have higher potential to simulate complex flows, have been used here. Also, the shear stress transport (SST; k-ω/k-ε) turbulence model was used for calculating the turbulent diffusivity in the Reynolds stress transport equation. The RSM Equations are:

$$\frac{\partial}{\partial t}\left(\rho\overline{u_i u_j}\right) + \frac{\partial}{\partial x_k}\left(\rho\overline{U_k}\,\overline{u_i u_j}\right) = -\frac{\partial}{\partial x_k}\left[\rho\overline{u_i u_j u_k} + \overline{p\left(\delta_{kj}u_i + \delta_{ik}u_j\right)}\right] +$$

$$\frac{\partial}{\partial x_k}\left[\mu\frac{\partial}{\partial x_k}\left(\overline{u_i u_j}\right)\right] - \rho\left(\overline{u_i u_k}\frac{\partial \overline{U_j}}{\partial x_k} + \overline{u_j u_k}\frac{\partial \overline{U_i}}{\partial x_k}\right) + p\left(\overline{\frac{\partial u_i}{\partial x_j}} + \overline{\frac{\partial u_j}{\partial x_i}}\right)$$

$$-2\mu\overline{\frac{\partial u_i}{\partial x_k}\frac{\partial u_j}{\partial x_k}} - 2\rho\Omega_k\left(\overline{u_j u_m}\varepsilon_{ikm} + \overline{u_i u_m}\varepsilon_{jkm}\right).$$

While, the SST equations are:

$$\frac{D\rho k}{Dt} = \tau_{ij}\frac{\partial \overline{U_i}}{\partial x_j} - \beta^*\rho\omega k + \frac{\partial}{\partial x_j}\left[\left(\mu + \sigma_k\mu_t\right)\frac{\partial k}{\partial x_j}\right]$$

$$+ 2\rho(1-F1)\sigma_{\omega 2}\frac{1}{\omega}\frac{\partial k}{\partial x_j}\frac{\partial \omega}{\partial x_j},$$

$$\frac{D\rho\omega}{Dt} = \frac{\gamma}{\nu_t}\tau_{ij}\frac{\partial \overline{U_i}}{\partial x_j} - \beta\rho\omega^2 + \frac{\partial}{\partial x_j}\left[\left(\mu + \sigma_\omega\mu_t\right)\frac{\partial \omega}{\partial x_j}\right].$$

More details of the terms are presented in references [9 and10].

5 Boundary Conditions

In all cases studied here, four different boundary conditions were used (Fig. 1a), namely, inflow, outflow, periodic, and no slip. Also, adiabatic wall condition was used in the energy equation. At the cross flow inflow boundary, up to 2D from the wall, the 1/7 power law was used. While, uniform flow was considered for the rest of the flow there. The square root of turbulent kinetic energy at the inflow boundaries was based on Ajersch et al. experimental data [6] and was $0.012V_{CF}$. While, ε was calculated from the following relation:

$$\varepsilon = C_\mu^{\frac{1}{4}}\frac{k^{\frac{3}{2}}}{l}, \quad l = 0.07L, \quad C_\mu = 0.09 \quad .$$

For RSM turbulence model, the Reynolds stress terms were prescribed as in references [6 and 10].

6 Computational Methodology

In this work, for simulation of the optimal 30° jet injection angle, the STAR-CD CFD code was used, which implements an implicit cell centered finite volume method [11]. Also, the SIMPLE algorithm (with under-relaxation coefficients) was used in the overall discretization of the equations. Note, all schemes used were second order. For the 90° jet injection angle case, in order to use Reynolds Stress Model, a CFD code (CFDARI) was developed. In this code, the Reynolds stress transport equations incorporated with SST model was used to close the equations. The method was control-volume using hybrid scheme. In order to link the mass and momentum equations, the SIMPLE algorithm was used. The other scalar quantities, such as k-ε and Reynolds stress terms, are segregately solved. To avoid the pressure checkerboard problem, a staggered grid arrangement with velocity component stored at the cell faces and all other scalar quantities located at the grid points was used. The system of equations was solved using a tridiagonal matrix algorithm employing an under-relaxation parameter to accelerate the convergence. Because of the importance of the inlet jet profile into the cross-flow domain, the flow field in the jet channel was also solved to derive a realistic profile in the jet exit.

7 Code Validation

To validate the code, velocity results obtained from our simulation (using both STAR-CD commercial and CFDARI codes) were compared with those of the available experimental and computational data of Ajersh et al. [6] for velocity ratio of 0.5 at the jet injection angle of 90° (Fig. 2). These comparisons show high accuracy of our simulations. Note, the quality and the accuracy of our results are much better than those of the computational results of Ajersch et al [6].

8 Results

In this work, flow physics and the film cooling effectiveness and efficiency were computationally studied for an incompressible stationary turbulent jets-into-cross flow over a flat plate. Different jet cross section's aspect ratio and two different jet injection angles (30° and 90°) at the velocity ratio of 0.5 were used. Note, as it is shown in reference [12], for both injection angles studied, the optimum velocity ratio is 0.5. In fact, for higher velocity ratios, the height of cooled flow increases and thus the region above the wall is more influenced by the cooling flow (which is against the main purpose of film cooling). On the other hand, for lower velocity ratios, the film cooling effectiveness on the wall decreases.

8.1 Flow Physics

As it is explained in reference [12], in film cooling phenomena, for injection angle of about 30º, the cooled fluid moves close to the wall (Fig. 3) and by increasing the jet injection angle to 90°, the height of the jets increases considerably, which is accompanied with highly rotational flow behind the jets. In fact, because of the flow three-dimensionality, the cold fluid behind the jets traps in one of the two symmetrical spirals which are moving along the wall downstream (Fig. 4). At this angle, there is also a small region of reverse flow just behind the jet and below the spiral flow, which creates a wake region at the wall (Fig. 5). Therefore, at 30° injection angle, the cold fluid has cooled the wall more efficiently without considerable influence on the flow far from the wall. In spite of the disadvantages of using 90° injection angle, it has some advantages. It is not only simpler for manufacturing purposes, it generates a wider distribution of film cooling in spanwise direction [12]. However, since the value of film cooling effectiveness along the spanwise direction is small, this advantage is not so important.

8.2 Film Cooling Effectiveness and Efficiency

In order to investigate the effects of the jet cross section's aspect ratio on film cooling effectiveness and efficiency, the results of a squared cross section and two different rectangular cross sections have been compared at the optimum velocity ratio of 0.5 and the jet injection angles of 30° and 90°. Figure 6 shows that, at the jet injection angle of 30°, changing the jet cross section from spanwise rectangle (case A) to square (case B) and also from square to streamwise rectangle (case C), decreases the effective film cooling length along the wall. At the jet injection angle of 90°, by changing the cross section from the spanwise rectangle (case A) to the streamwise rectangle (case C), the length of cooled flow on the wall decrease too (Fig.7). However, comparing the results of 30° and 90° in each jet cross section (Fig's. 6 and 7) shows the extreme decrease of film cooling effectiveness length along the wall when going from 30° to 90°.

Furthermore, at 30° jet injection angle, by changing the jet cross section from spanwise rectangle (case A) to streamwise rectangle (case C), the height of cooled flow behind the jet is increased and thus the fluid far from the wall also cools down (Fig. 8). In other words, the film cooling affects mostly the main flow rather than the fluid adjacent to the wall. This is also true for the jet injection angle of 90° (Fig.9). At this angle, the influence of cooled flow to the mainstream increases by changing the jet cross section from spanwise rectangle (case A) to streamwise rectangle (case C). This figure also shows that, the height of spiral's center to the jet spacing (4.5D) is 5.3%, 6.98%, and 8.5% at the jets cross sections of spanwise rectangle (case A), square (case B), and streamwise rectangle (case C), respectively. Comparing the film cooling effectiveness contour of 30° and 90° jet injection angles at each jet cross section, shows the higher influence of the cooled flow at 90° than that of 30°.

Figure 10 shows that, at the jet injection angle of 30°, changing the cross section from spanwise rectangle (case A) to the streamwise rectangle (case C) decrease the cooled region on the wall. In fact, the spanwise rectangle (case A) not only cools a wider region in spanwise direction (because of its geometry), but also can cool a wider region in streamwise direction. This is also valid for jet injection angle of 90° (Fig. 11). In fact, changing the jet cross section from spanwise rectangle (case A) to streamwise rectangle (case C) decrease the cold region along the wall. Of course, comparing the contours of 30° and 90° at each jet, indicates the considerable decrease of film cooling along the wall by increasing the jet injection angle.

Figure 12 shows the film cooling effectiveness at the centerline of all three spanwise rectangle, square, and streamwise rectangle at the jet injection angle of 30° and 90°. This figure confirms that, changing the cross section from spanwise rectangle (case A) to streamwise rectangle (case C) or changing the jet injection angle from 30° to 90° decreases the film cooling effectiveness.

Figure 13 shows the film cooling effectiveness at position X=0.09 at the wall. Again, this figure confirms that, changing the cross section from spanwise rectangle (case A) to streamwise rectangle (case C) decreases the film cooling effectiveness at both angles of 30° and 90°. Comparing the results of these two angles indicates that, increasing the jet angle decreases the maximum film cooling effectiveness, but generates a wider distribution of film cooling in spanwise direction.

Another important point noticed in figures 12 and 13, (especially at 30° injection angle) is that, although the length and the width of both spanwise and streamwise rectangular jets (cases A and C) are the same, the differences between the results of the spanwise rectangular jet (case A) and the squared one (case B) is more than that of the streamwise rectangular jet (case C) and the squared one (case B). In fact, the more the rectangular section stretches in the spanwise direction, the more rapidly the effectiveness increases.

Another point is that, at the injection angle of 30°, in spanwise rectangular jet (case A), the film cooling effectiveness is reduced from unity just as the cold fluid crosses the jet. While, at the same time, the streamwise rectangular jets (case C) can sustain film cooling effectiveness of unity at longer distances. However, after that, the film cooling effectiveness of the streamwise rectangular jet (case C) decreases quickly, while the rate of decrease in spanwise rectangular jet (case A) is much lower.

9 Conclusion

In this work, the effects of the jet cross-section's aspect ratio were investigated for an incompressible stationary turbulent jets-into-cross flow over a flat plate at the optimal velocity ratio of 0.5. The results show that, at both jet injection angles of 30° and 90°, changing the jet cross section from spanwise rectangle to streamwise rectangle decreases the effective film cooling along both streamwise and spanwise directions. Also, it increases the height of the cooled flow behind the jet. Thus, the flow far from the wall becomes cool resulting in higher aerodynamic losses. In addition, at the injection angle of 30°, the more the rectangular section stretches in spanwise direction, the more rapidly the cooling effectiveness increases.

References:

[1] Oates, G., *Aerothermodynamics of Aircraft Engine Components*, AIAA Education Series, AIAA, 1985.

[2] Cho, H., Kang, S., and Rhee, D. H., "Heat/Mass Transfer Measurement Within a Film Cooling Hole of Square and Rectangular Cross Section," *ASME Turbo Expo 2001 Conference*, American Society of Mechanical Engineering (ASME), New Orleans, USA, 2001.

[3] Gartshore, I., Salcudean, M., and Hassan, I., "Film Cooling Injection Hole Geometry: Hole Shape Comparison for Compound Cooling Orientation," *AIAA Journal*, Vol. 39, No. 8, 2001, pp. 1493-1499.

[4] Muldoon, F., and Acharya, S., "Numerical Investigation of the Dynamical Behavior of a Row of Square Jets in Cross Flow Over a Surface," *ASME Turbo Expo 1999 Conference*, Paper No. 99-GT-127, American Society of Mechanical Engineering (ASME), Indiana, USA, 1999.

[5] Licu, D. N., Findlay, M., Gartshore, I., and Salcudean, M., "Transient Heat Transfer Measurements Using a Single Wide-Band Liquid Crystal Test," *ASME Journal of Turbomachinery*, Vol. 122, No. 3, 2000, pp. 546-552.

[6] Ajersch, P., Zhou, J. M., Ketler, S., Salcudean, M., and Gartshore, I. S., "Multiple Jets in a Cross-Flow: Detailed Measurements and Numerical Simulations," *International Gas Turbine and Aeroengine Congress & Exposition*, Paper No. 95-GT-9, American Society of Mechanical Engineering (ASME), Houston, Texas, USA, 1995.

[7] Launder, B. E., and Spalding, D. B., *Lectures in Mathematical Models of Turbulence*, Academic Press, London, England, 1972.

[8] Launder, B. E., and Spalding, D. B., "The Numerical Computation of Turbulent Flows," *Journal of Computer Methods in Applied Mechanics and Engineering*, Vol. 3, 1974, pp. 269-289.

[9] Keimasi, M. R., and Taeibi-Rahni, M., "Numerical Simulation of Jets in a Cross-Flow Using Different Turbulence Models," *AIAA Journal*, Vol. 39, No. 12, 2001, pp. 2268-2277.

[10] Javadi, A., Javadi, K., Taeibi-Rahni M., and Keimasi M., (2002) "Reynolds Stress Turbulence Models for Prediction of Shear Stress Terms in Cross Flow Film Cooling – Numerical Simulation,"4th International ASME/JSME/KSME Conference, Canada.

[11] Anon., *Methodology: STAR-CD Version 3.15*, Computational Dynamics Limited, UK, 2001.

[12] Mahjoob, S., Taeibi_Rahni, M. "Parameters Affecting Turbulent Film Cooling- RANS Computational Simulation", Accepted for Publication in *Journal of Thermophysics and Heat Transfe*r, AIAA.

[13] Fric, T.F. and Roshko, A., "Vortical Structure in the Wake of a Transverse Jet," *Journal of Fluid Mechanics*, Vol. 279, 1994.

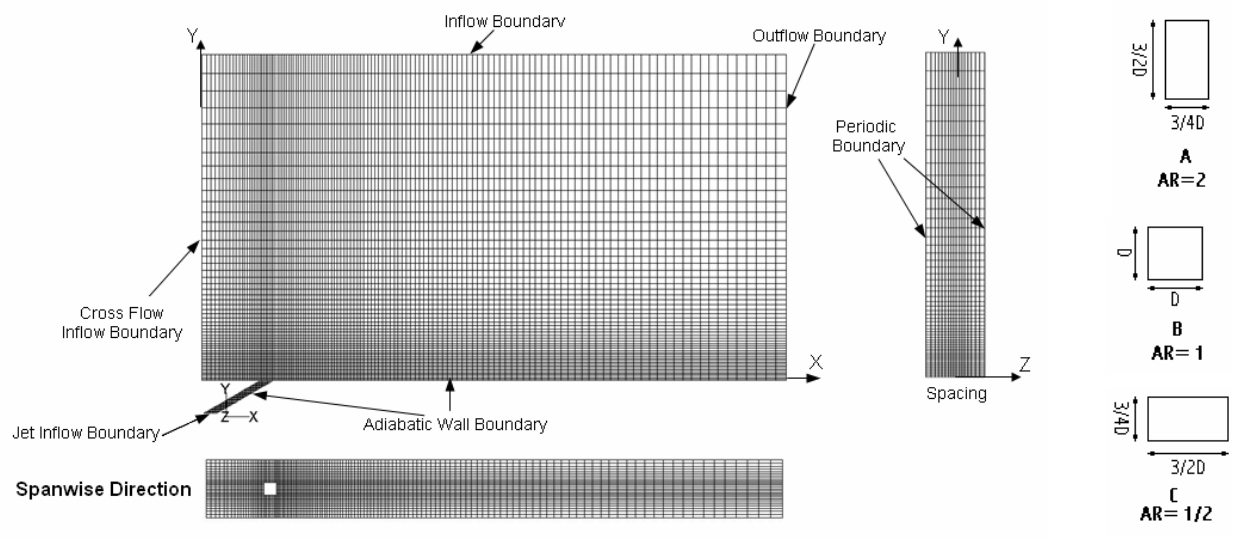

Fig.1 The geometric modeling and the boundary conditions used: (a) grid and boundary conditions in basic domain and (b) different jet cross sections (AR: aspect ratio).

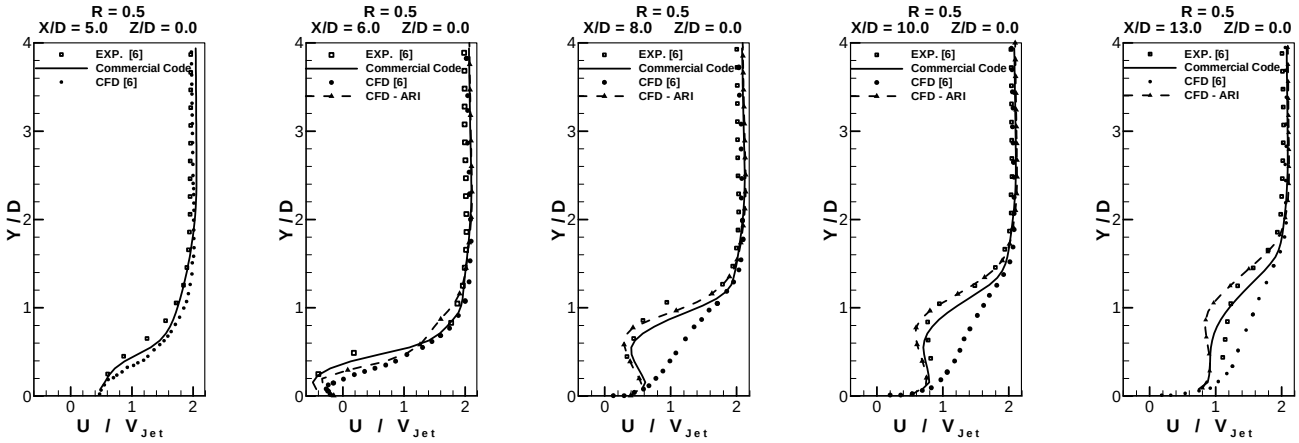

Fig.2 Comparison of streamwise velocity (U/V_{Jet}) for Z/D=0, with velocity ratio (R) of 0.5 and jet injection angle of 90° a) X/D=5.0, b) X/D=6.0, c) X/D=8.0, d) X/D=10.0, and e) X/D=13.0.

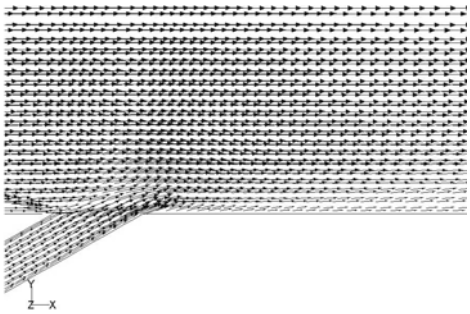

Fig.3 Flow velocity vectors near the wall at Z=0, at the jet injection angle of 30° and R= 0.5.

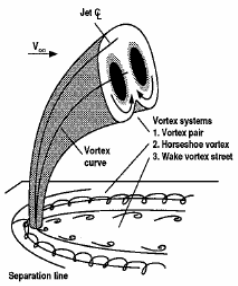

Fig.4 Different vortices generated in jet injection angle of 90° [13].

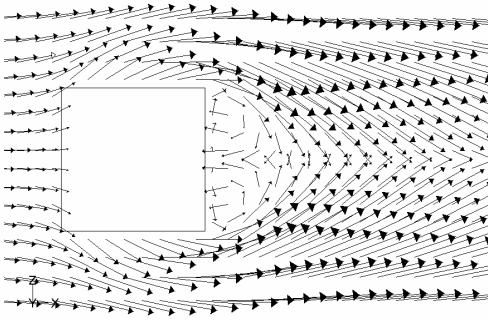

Fig.5 Wall wake for the jet injection of 90° and R= 0.5, using discrete hole injection.

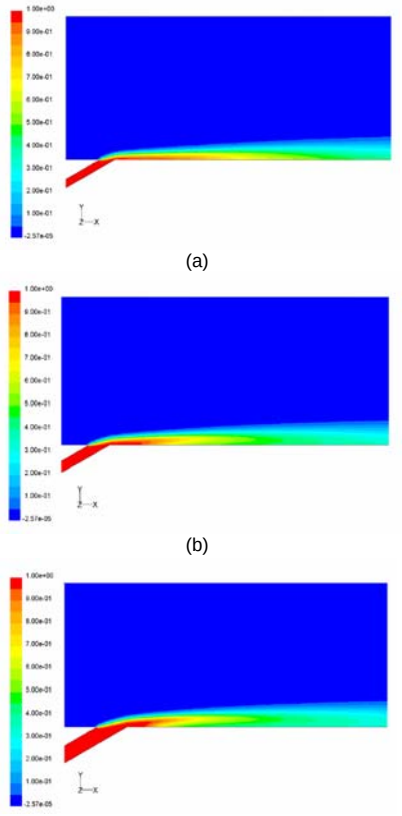

Fig.6 Film cooling efficiency contour at Z=0 and jet injection angle of 30°, for different jet cross sections, (a) spanwise rectangular jet, (b) squared jet, and (c) streamwise rectangular jet.

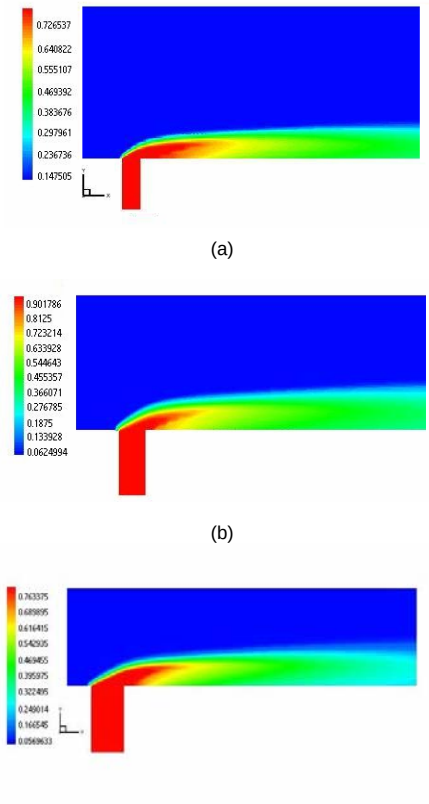

Fig.7 Film cooling efficiency contour at Z=0 and jet injection angle of 90°, for different jet cross sections, (a) spanwise rectangular jet, (b) squared jet, and (c) streamwise rectangular jet.

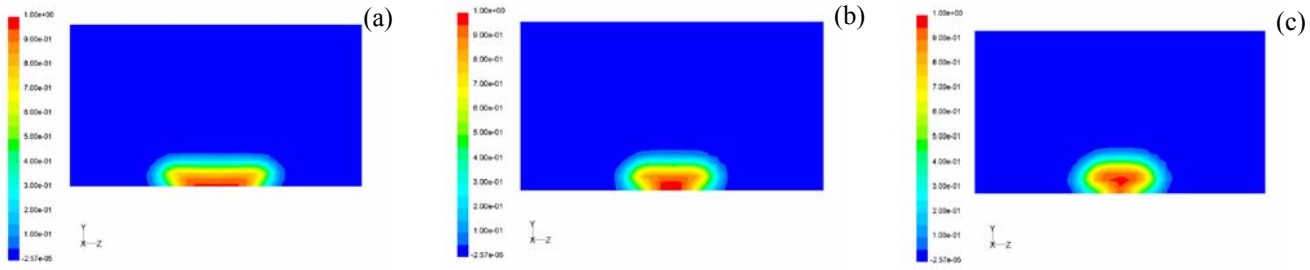

Fig.8 Film cooling efficiency contour at the position of 1D behind each jet and jet injection angle of 30°, for different jet cross sections, (a) spanwise rectangular jet, (b) squared jet, and (c) streamwise rectangular jet.

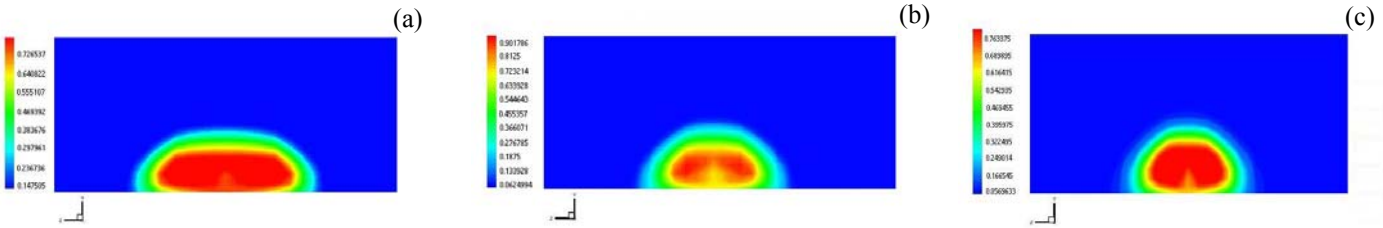

Fig. 9 Film cooling efficiency contour at the position of 1D behind each jet and jet injection angle of 90°, for different jet cross sections, (a) spanwise rectangular jet, (b) squared jet, and (c) streamwise rectangular jet.

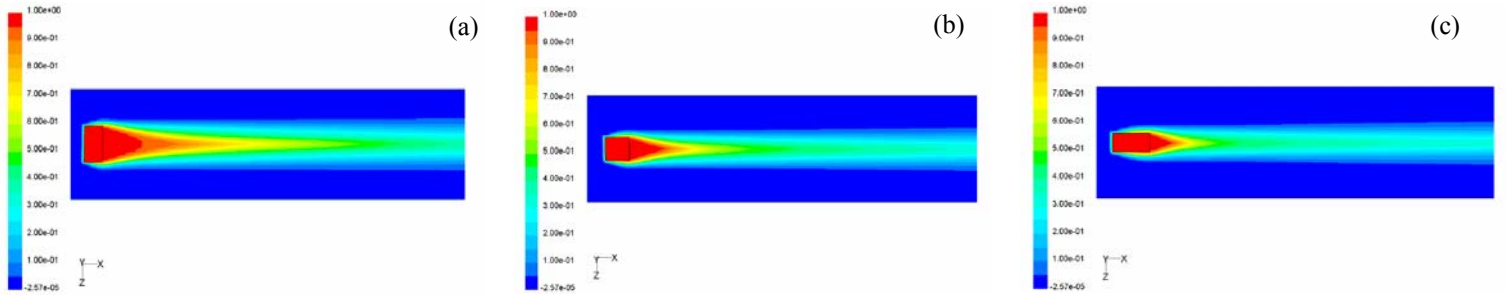

Fig.10 Film cooling effectiveness contour on the wall and jet injection angle of 30°, for different jet cross sections, (a) spanwise rectangular jet, (b) squared jet, and (c) streamwise rectangular jet.

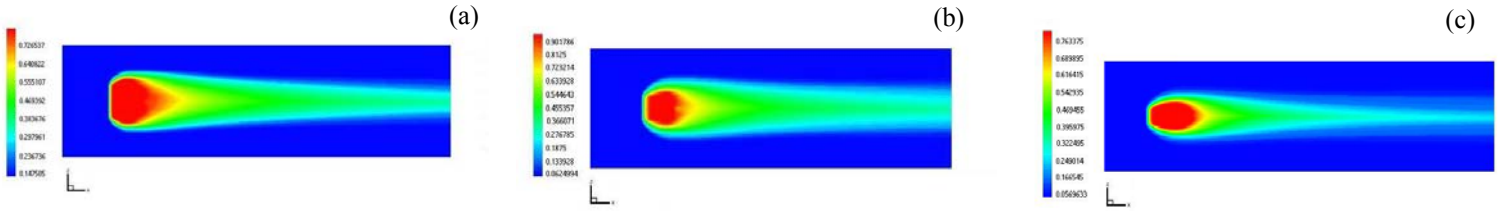

Fig.11 Film cooling effectiveness contour on the wall and jet injection angle of 90°, for different jet cross sections, (a) spanwise rectangular jet, (b) squared jet, and (c) streamwise rectangular jet.

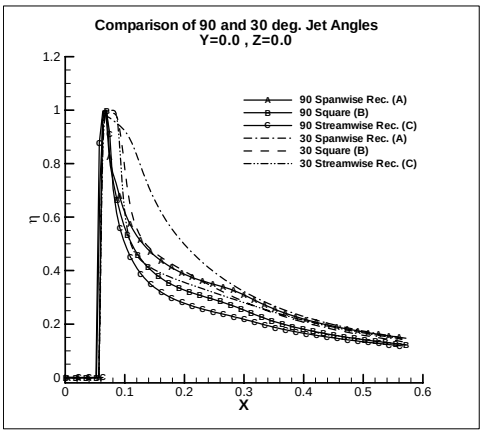

Fig.12 The film cooling effectiveness at the jet centerline (Y=0 and Z=0), for different jet aspect ratios at the jet injection angles of 30° and 90°.

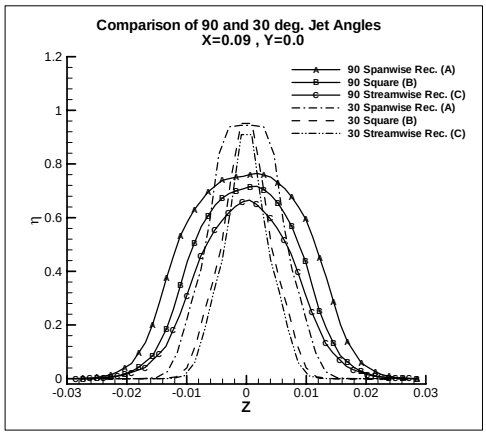

Fig.13 The film cooling effectiveness at X=0.09 on the wall, for different jet aspect ratios at the jet injection angles of 30° and 90°.